INFLUENCE OF MICROSTRUCTURE ON FRACTURE PROPAGATION IN ROCK

Richard G. Hoagland, et al

Battelle Columbus Laboratories

Prepared for:

Advanced Research Projects Agency
Bureau of Mines

October 1973

Unclassified

Security Classification

AD 774 145

DOCUMENT CONTROL DATA - R & D

(Security classification of title, body of abstract and indexing annotation must be entered when the overall report is classified)

1. ORIGINATING ACTIVITY (Corporate author)

Battelle, Columbus Laboratories
505 King Avenue
Columbus, Ohio 43201

2a. REPORT SECURITY CLASSIFICATION: Unclassified

2b. GROUP:

3. REPORT TITLE

Influence of Microstructure on Fracture Propagation in Rock

4. DESCRIPTIVE NOTES (Type of report and inclusive dates)

Final Technical Report for period May 12, 1972 to June 1, 1973

5. AUTHOR(S) (First name, middle initial, last name)

R. G. Hoagland, G. T. Hahn, and A. R. Rosenfield

6. REPORT DATE: October, 1973

7a. TOTAL NO. OF PAGES: 40

7b. NO. OF REFS: 20

8a. CONTRACT OR GRANT NO: H0220066

b. PROJECT NO. ARPA Order No. 1579
Amendment No. 3
c. Program Code No. 2F10

d.

9a. ORIGINATOR'S REPORT NUMBER(S): None

9b. OTHER REPORT NO(S) (Any other numbers that may be assigned this report): None

10. DISTRIBUTION STATEMENT

Distribution of this document is unlimited

11. SUPPLEMENTARY NOTES

12. SPONSORING MILITARY ACTIVITY

Advanced Research Project Agency
1400 Wilson Blvd.
Arlington, Va. 22209

13. ABSTRACT

This report describes the results of research to measure the tensile fracture resistance and identify the mechanism of fracture in three rock types: Barre granite, Sioux quartzite, and Dresser basalt. The method involved wedge-loading of double-cantilever-beam specimens from which the fracture energy dissipation rate, R, was determined. The specimen orientation and environment were varied in the tests. In addition, the specimens were monitored for acoustic emissions during the tests and fractography was performed on selected broken specimens by optical, scanning electron and electron microscopy of two-stage replicas. In all three rock types the crack was observed to propagate in a slow stable manner. The best characterization of the R measurements is the large degree of data scatter. This scatter was most severe in the basalt and the presence of large preexisting flaws in this material are suspected. A comparison of fracture energy for fracture parallel to the rift, grain, and hardway planes in the granite showed no effect of orientation. Some orientation dependence was observed, however, in the quartzite and basalt. Also comparison of fracture energies from tests in air, 500 ppmw $AlCl_3$ solution and liquid nitrogen showed no distinct effect of environment or test temperature. For all orientations and test conditions the R values for the granite are 150 to 338 J/m^2, for the quartzite 71 to 1178 J/m^2, and for the basalt, 240 to 3011 J/m^2. Prior to crack extension acoustic activity was detected in the granite and quartzite. This observation together with the nonlinear load-displacement records and the fractography provide evidence for extensive microcracking. As in previous work on limestone and sandstone, microcrack formation is considered to be the principal energy dissipating mechanism during fracture to the extent that it affords a means of dissipating roughly 100 times more energy per unit projected area than the intrinsic surface energies of the constitutents. In the basalt the situation is more uncertain but microcracking is considered to be the most likely energy dissipating mechanism.

DD FORM 1 NOV 65 1473

Unclassified

Security Classification

49

14. KEY WORDS	LINK A		LINK B		LINK C	
	ROLE	WT	ROLE	WT	ROLE	WT
Rock Mehcanics						
Rock Fracture						
Fracture Mechanics						
Microstructure						
Fractography						
Microcracking						
Granite						
Basalt						
Quartzite						

FINAL REPORT

on

INFLUENCE OF MICROSTRUCTURE ON FRACTURE PROPAGATION IN ROCK

by

R. G. Hoagland
G. T. Hahn, Principal Investigator
A. R. Rosenfield
(614-299-3151)

October, 1973

to

BUREAU OF MINES
Twin Cities Research Center
Mr. George Savanick, Project Engineer, 612-725-4597

Contract No. H0220066

Sponsored by
Advanced Research Projects Agency
ARPA Order No. 1579, Amend. No. 3
Program Code No. 2F10

Contract Date: May 12, 1972 to June 1, 1973

Contract Amount $44,840

ib

BATTELLE
Columbus Laboratories
505 King Avenue
Columbus, Ohio 43201

TABLE OF CONTENTS

	Page
TECHNICAL REPORT SUMMARY	i
INTRODUCTION	1
EXPERIMENTAL PROCEDURES	4
Materials	4
Testing Methods	5
RESULTS	11
Fractography	19
Effect of Specimen Size on R	28
DISCUSSION	30
CONCLUSIONS	38
REFERENCES	39
APPENDIX A	A-1

TECHNICAL REPORT SUMMARY

This report describes the results of research to measure the tensile fracture resistance and identify the micro-mechanism of fracture in three rock types: Barre granite, Sioux quartzite, and Dresser basalt. The experiments involved wedge-loading of double-cantilever-beam specimens from which the fracture energy dissipation rate, R, was determined. The specimen orientation and environment were varied in the tests. In addition to measurement of load/displacement records, the specimens were monitored for acoustic emissions during the tests and the fracture surfaces of selected broken specimens were examined by optical-, scanning-electron-, and replica-electron-microscopy.

In all three rock types the crack was observed to propagate in a slow stable manner. The most striking feature of the energy dissipation rate measurements is the large degree of data scatter. This scatter was most severe in the basalt and the presence of large preexisting flaws in this material are suspected. A comparison of fracture energy for fracture parallel to the rift, grain, and hardway planes in the granite showed no effect of orientation. Some orientation dependence was observed, however, in the quartzite and basalt. Also comparison of fracture energies from tests in air, 500 ppmw $AlCl_3$ solution and liquid nitrogen showed no distinct effect of environment or test temperature. For all orientations and test conditions the R values for the granite are 150 to 338 J/m^2, for the quartzite 71 to 1178J/m^2, and for the basalt, 240 to 3011 J/m^2.

Prior to crack extension acoustic activity was detected in the granite and quartzite. This observation together with the nonlinear load-

displacement records and the fractography provide evidence for extensive microcracking. As in previous work on limestone and sandstone, microcrack formation is considered to be the principal energy dissipating mechanism during fracture to the extent in that it affords a means of dissipating roughly 100 times more energy per unit projected fracture area than the intrinsic surface energies of the constituents. In the basalt the situation is more uncertain but microcracking is considered to be the most likely energy dissipating mechanism.

The methods used in this research not only describe the sources of fracture resistance in rocks but are sufficiently general to be applied to other ceramic materials. In particular, the microcrack model developed to analyze nonlinearities in the load/displacement curves, suggests that fine-grained ceramics are tougher than coarse-grained ceramics. Development of superior materials can be aided by this result.

FINAL REPORT

on

INFLUENCE OF MICROSTRUCTURE ON FRACTURE PROPAGATION IN ROCK

by

R. G. Hoagland
G. T. Hahn, Principal Investigator
A. R. Rosenfield

INTRODUCTION

Failure criteria for rock and brittle polycrystalline ceramics (of which most rocks are a special class) have proven difficult to quantify. Even the tensile strength of rocks is an illusive quantity. In a recent report, Fairhurst[1] shows that the tensile strength of rocks may be dependent on the type of test employed in its measurement. Furthermore, there is evidence, although inconclusive, that the tensile strength is volume dependent. Work in this laboratory and others suggests that the failure of rocks under tension occurs principally as a gradual formation of microcracks. The volume and stress gradient dependence of the density and distribution of microcracks may provide some explanation of these results. It thus appears that the characterization of the strength of these materials can not be made without a clear understanding of the failure mechanisms.

One measure of fracture resistance is the fracture energy dissipation rate. This quantity, R, is defined as the increment of work consumed in extending a crack a unit distance in a test piece of unit thickness

(creating two units of surface area) and is related to G, the corresponding elastic energy release rate† (by the classical Griffith arguments; R ≡ G) provided the crack speed is small so that the kinetic energy content in the specimen is of no concern. Previous work[2,3] on Indiana limestone and Berea sandstone revealed that R for fracture of these rocks was several orders of magnitude greater than the intrinsic surface energy of calcite.†† While plastic deformation in the highly stressed region surrounding the crack tip could account for this high energy dissipation rate, this possibility was eventually discarded. Acoustic emission during the tests, increased permeability near the crack front, and tests at low temperatures led to the conclusion that microcracking is the important and possibly the only, energy dissipative mechanism. This model provides the explanation for spurious tensile strength data as noted earlier In addition, by analogy with the crack tip plastic zone in metals, and the limitations this imposes on the application of fracture mechanics, the very large discrepancy between measured tensile strength and strength of rocks calculated using simple Griffith theory could be explained.[2,3] The results are supported by the work of other researchers notably Moavenzadeh and Kuguel[4], Friedman and coworkers[5] and Fairhurst[1].

The measurement of R during fracture in limestone and sandstone provided a useful method for interpreting fracture mechanisms in these

---

† $G \equiv \left(\frac{dW}{dA} - \frac{dU}{dA}\right)$, where W is the work exchanged between the test piece and the surroundings, U is the elastic strain energy in the specimen, and A is the projected area of one fracture surface.

†† Fracture occurs within the calcite phase in both materials. The intrinsic R for calcite is 0.5 J/m^2 while R values as high as 1580 J/m^2 were recorded.

materials. This report describes the subsequent years effort to extend the technique to the measurement of R in three harder and microstructurally more complex rocks; namely, Barre granite, Dresser basalt and Sioux quartzite. The wedge-loaded double-cantilever-beam test developed for R measurements on the limestone and sandstone was successfully applied. Tests were conducted at room temperature and at -196°C. In addition, many of the tests at room temperature included acoustic emission measurements. Fractography of selected fracture areas was conducted principally on the granite and basalt using optical microscopy scanning electron microscopy and electron microscopy of two-stage replicas. These experiments sought to answer the following questions:

- Is R an anisotropic quantity, and, if so, does the anisotropy relate to the microstructural fabric?
- What is the evidence of microcracking during fracture in these rocks?
- Does the fracture energy involve work done by processes other than microcracking such as by dislocation generation and motion?
- Is R sensitive to environment?

The latter point was investigated by comparison of R results from tests in air, distilled water and 500 ppmw $AlCl_3$ solutions.

Finally, the development of an extensively microcracked zone surrounding the crack tip may invalidate the method for deriving R from the test parameters if the zone becomes large compared to the specimen dimension. This possibility may have influenced the results derived from the previous tests on limestone and sandstone. Therefore, some additional tests in which the specimen size was varied were also conducted. These

tests were confined to Berea sandstone since a size effect, if it exists, should be prominent due to the apparent ease of microcrack formation in this material.

EXPERIMENTAL PROCEDURES

Materials

Blocks of Barre granite, Dresser basalt, and Sioux quartzite measuring approximately one foot (31 cm) on a side were obtained from the U. S. Bureau of Mines. These rocks are part of a standardized suite for use by ARPA contractors. The granite, basalt and quartzite were obtained from Barre, Vt., Dresser, Wis., and Jasper, Minn., respectively.

Based on analyses by Douglass and Voight[6] and Krech[7], Barre granite contains approximately 22 per cent to 25 per cent quartz. The relative abundance of potash feldspars and plagioclase differ as reported by these investigations. Douglass and Voight report 20% potash feldspars and 35% plagioclase while Krech reports 10% and 50% for the same constituents. The remaining constituents are approximately 6 to 9 per cent each of biotite and muscovite. Three orthogonal planes are identified in Barre granite as a result of quarrying experience: the rift, a nearly vertical plane with a strike of N32°E, the grain, a nearly horizontal plane; and the hardway, perpendicular to the other two. Douglass and Voight found a preponderance of planar microcracks in the quartz phase with normals nearly parallel to the rift pole and, to a lesser degree, parallel to the grain pole.

The Sioux quartzite is a dense pink rock containing approximately 99% quartz. White to light pink lamellae 1 to 5 mm thick and oriented parallel to the horizontal plane were apparent.

The constitutents in the Dresser basalt were identified by Krech[7]. The microstructure is characterized generally by a duplex grain structure of black grains 0.1 to 0.5 mm diameter and approximately 5 mm diameter contained in a green matrix. The phases are principally plagioclase (41%) and pyroxene (40%). Macroscopically this rock displays isotropic texture. The presence of large, very weak interfaces or cracks is suspected in the samples obtained as a number of specimens fell apart during the cutting or grinding operations.

The fourth rock, Berea sandstone has been described elsewhere.[2,3]

Groups of test specimens were cut from each of the three hard rocks such that, in each group, the crack plane was parallel to one of the cube faces. In addition, in several of the groups, specimens with different orientations were cut in order to vary the direction of crack propagation. The crack planes and crack propagation directions for the three hard rocks are identified schematically in Figure 1.

Testing Methods.

The fracture energy dissipation rate R, was obtained by means of the wedge-loaded double-cantilever-beam test. As this test has been described in detail elsewhere[2,3] only a brief summary of the method is given here.

The specimen geometry and approximate dimensions are given in Figure 2. The specimens were prepared by sawing, in kerosene (except for the sandstone which was cut in water), followed by grinding to the finished size. The specimen is loaded by forcing a wedge between pins inserted into the steel tabs which, in turn, are glued to the ends of the specimen. As

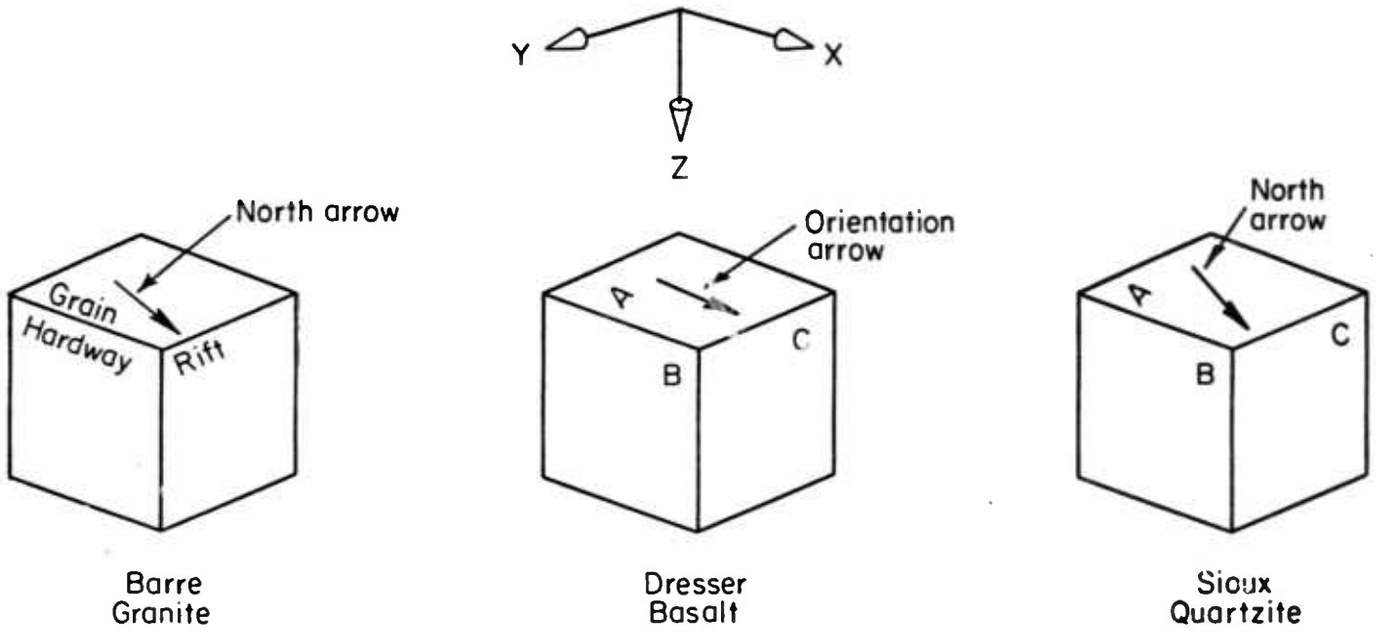

FIGURE 1. ROCK CUBES OBTAINED FROM ARPA-USBM SUITE SHOWING RELATIVE ORIENTATION OF CRACK PLANES AND CRACK PROPAGATION DIRECTIONS. Several orientations of test specimens were cut from each cube to produce fracture surfaces parallel to each labeled face. The crack propagation direction is denoted by X, Y, or Z. The planes labeled "GRAIN" in the granite and "A" in the Quartzite are horizontal planes.

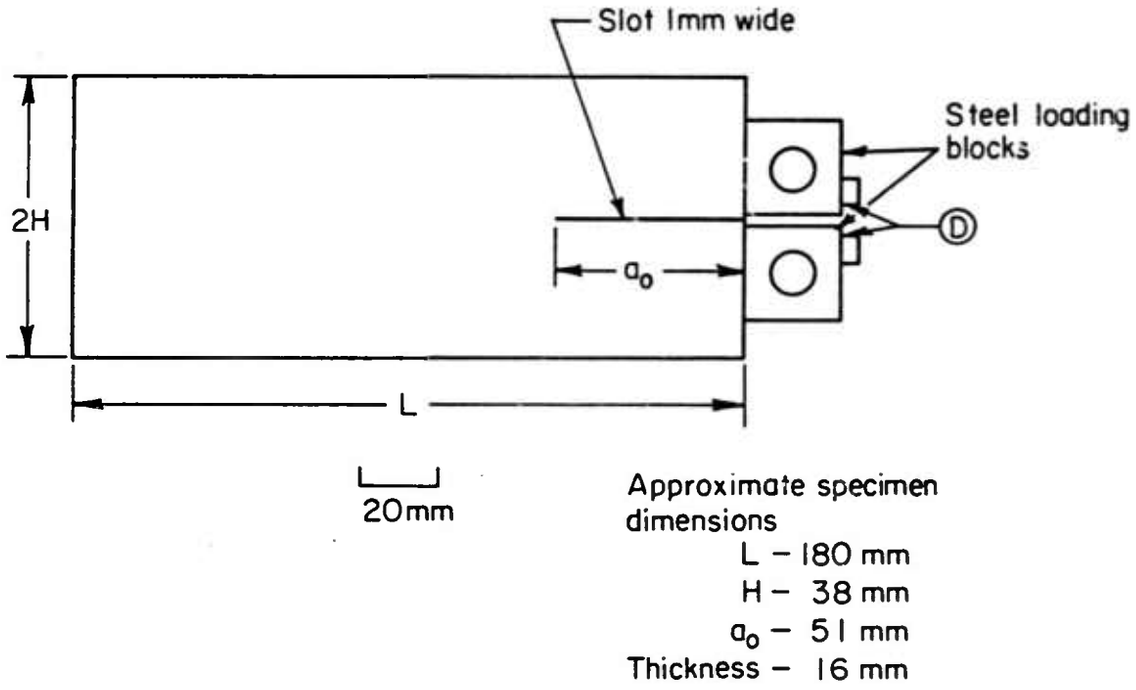

FIGURE 2. THE DOUBLE-CANTILEVER-BEAM SPECIMEN. Steel blocks containing 1/2-in. dia. pinholes are attached to the end of the specimen by means of an epoxy. During testing a clip gage monitors the relative displacement of the arms of the specimen at "D".

load is applied, the arms of the specimen are spread and the measurement of displacement at the tabs together with crack length allow calculation of R by the expression given below. The crack length is monitored as a result of the stepwise resistance change in a parallel array of conducting strips drawn on the specimen surface with a graphite pencil.

Using the usual relation between the strain energy release rate and stress intensity, i.e., $R = G \equiv K^2/E$, where E is Young's modulus and the identity applies to slow propagations (negligible kinetic energy), we derive from the stress intensity expressions of Kanninen[8] for the double-cantilever-beam geometry

$$R = \frac{3h^3 E \lambda^4 B^2 (\delta^2)}{4[2(\lambda a)^3 + 3A\lambda a + 3B]^2} \qquad (1)$$

where

$$A = \frac{\sinh^2\psi + \sin^2\psi + 2a\lambda\,(\sinh\psi\cosh\psi + \sin\psi\cos\psi)}{\sinh^2\psi - \sin^2\psi}$$

$$B = \frac{\sinh\psi\cosh\psi - \sin\psi\cos\psi + a\lambda\,(\sinh^2\psi + \sin^2\psi)}{\sinh^2\psi - \sin^2\psi}$$

$$\lambda = \frac{6^{1/4}}{h}$$

$\psi = \lambda\,(L-a)$

a = crack length

L = specimen length

h = beam height

δ = displacement of one beam relative to the other at the glue line between the tabs and specimen material.

The latter measurement is not obtained directly since the relative displacement of the beams is actually obtained from the end of the tabs. The

correction accounting for end rotation and thus necessary to obtain δ from the actual measured δ' is

$$\delta = \frac{\delta'}{1 + \frac{3\lambda d[(\lambda a)^2 + A]}{2(\lambda a)^3 + 3A\lambda a + 3B}} \qquad (2)$$

where d = distance from the end of the specimen (glue line) to the point at which δ' is measured.

The calculation of R from the crack length and displacement measurements requires the elastic modulus, E. The tensile moduli values obtained by Krech[7] for the ARPA suite of basalt, quartzite and granite were employed and these are given in Table 1.

TABLE 1. TENSILE YOUNG's MODULUS

	GN/m^2	(10^6 psi)
Basalt	119	(17.3)
Quartzite	27.9	(4.05)
Granite	17.5	(2.54)

There exists some uncertainty in the proper moduli values to use because of anisotropy. For example, Douglass and Voight report that Young's modulus for Barre granite varies by a factor of about two with the greatest compliance in the direction perpendicular to rift and the least compliance perpendicular to the hardway direction. As evidenced by the pulse velocity measurements of Krech[7] the elastic anisotropy of the basalt and quartzite is not as pronounced as in the granite.

It has been shown by Hoagland[9] that at fixed displacement the crack driving force, G, is a rather strongly decreasing function of crack length for this specimen geometry. This is a favorable characteristic of

the DCB specimen because, with moderate testing machine stiffness it is possible to achieve stable crack extension, i.e., crack growth occurring at a rate entirely dependent upon a rate of displacement of the beams, and thereby allow measurement of R at a large number of points on the crack path. All of the specimens tested displayed a degree of stable crack extension for some distance. As noted in the results in the stable crack growth regime, the crack extension process actually consists typically of a series of small but rapid increases in length. Each of these abrupt propagation events is unstable on a local or microscopic scale as for example fracture of a single crystallite. However, there is insufficient energy available to continue the expansion on the crack. In contrast, unstable propagation characteristically led to crack extension to the boundaries of the specimen. Crack extension typically became unstable when the crack tip wandered from the specimen midplane or advanced to a point near the end of the specimen. In the former case, one or both of the specimen arms are broken off. R values were considered valid only for that part of the crack path which deviated by no more than 0.1 H from the specimen midplane.* The compression supplied by the wedge tends to suppress the drift of the crack from the midplane. However, even with a relatively large wedge angle of 130° the crack eventually ran to the specimen side in approximately 75% of the tests. It is thought that this behavior is associated with weak interfaces or preexisting cracks of fairly large size.

Tests were conducted at room temperature (approximately 22°C) in air, distilled water, 500 ppmw $AlCl_3$ solutions, and in liquid nitrogen (-196°C). During the tests in air acoustic activity the specimens were

---

* H ≡ specimen half-height, see Figure 1.

monitored by means of Glennite PZT transversely sensitive crystals attached to a small brass block. The block was acoustically coupled to the specimen surface by means of a viscous resin. The signals were filtered to remove frequency components below 20 kHz and amplified by 1000 prior to counting. To minimize stray noise from the loading fixture the specimens were placed on a rubber pad on the loading platen and teflon sheets were used between the wedge and pins. Previous experience showed these precautions to be effective and, hence, the acoustic pulses registered by the recording equipment during an actual test originate in the bulk of the specimen, presumably in the region of high stress surrounding the slot tip.

RESULTS

Typical features of the mechanical behavior of the rock specimens during testing are displayed in Figures 3(a), (b), and (c). The Barre granite in Figure 3(a) begins to show detectable nonlinearity in the load-displacement record at about 1750 Newtons (~ 395 lbs) together with the first occurrence of acoustic activity. This departure from linearity may be either the result of a general decrease in the compliance of the specimen due to microcrack formation or the onset of crack extension. However, the growth of the crack starting from the tip of the saw cut is not evident until a load of about 2200 Newtons (495 lbs) is reached. The important features of the behavior displayed in this record which bears on the interpretation of the fracture mechanism is that some acoustic activity together with departure from linearity of the load-displacement record occur sometime prior to the onset of crack extension.

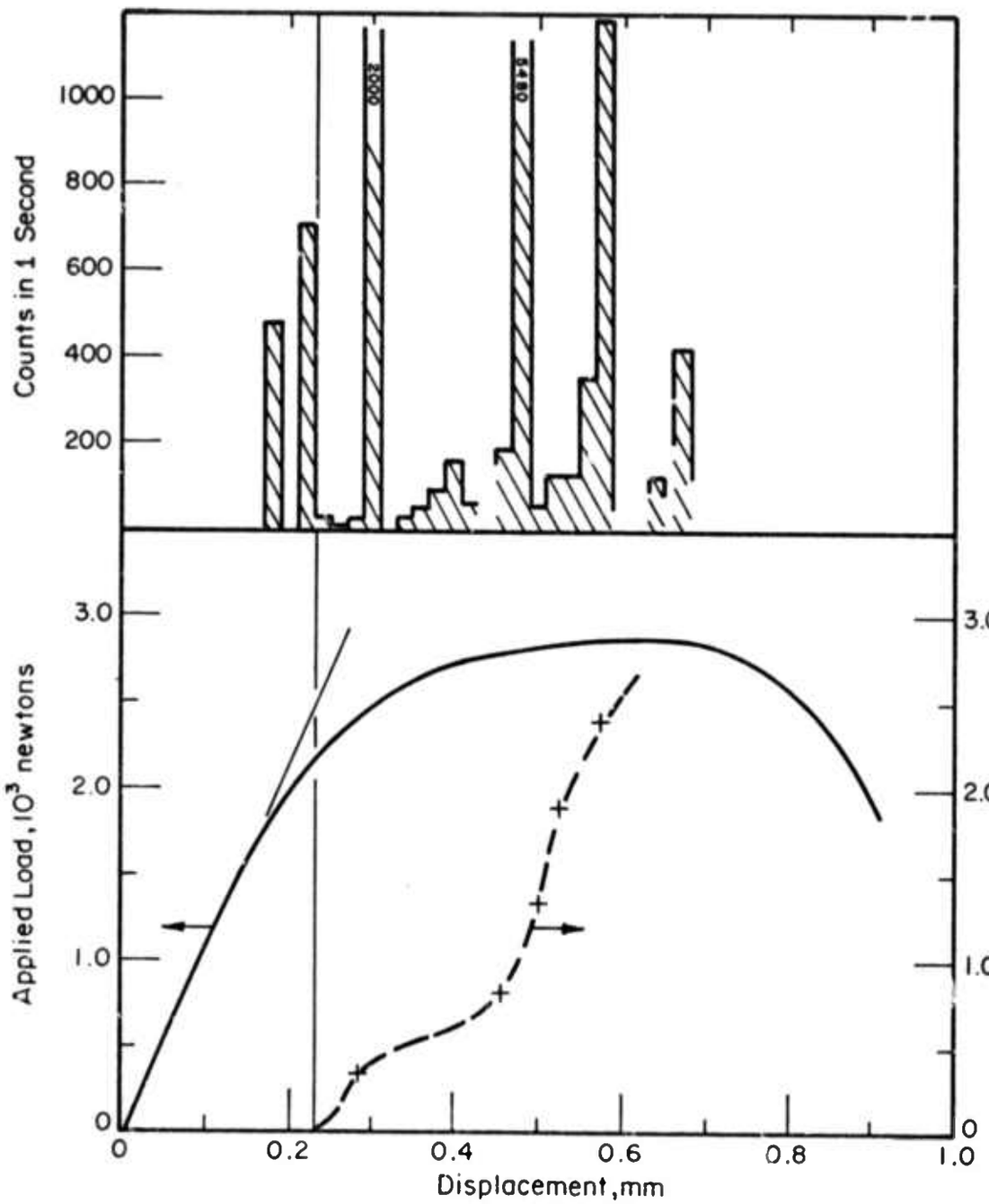

(a) Barre Granite (Specimen GHZ-2)

FIGURE 3. TYPICAL LOAD-DISPLACEMENT (BOTTOM) AND ACOUSTIC ACTIVITY RECORDS (TOP) FOR (a) BARRE GRANITE (SPECIMEN GHZ-2), (b) SIOUX QUARTZITE (SPECIMEN QAX-3) AND (c) DRESSER BASALT (SPECIMEN BAX-1). Note that some acoustic activity and nonlinear loading behavior is evident in (a) and (b) prior to onset of detectable crack extension.

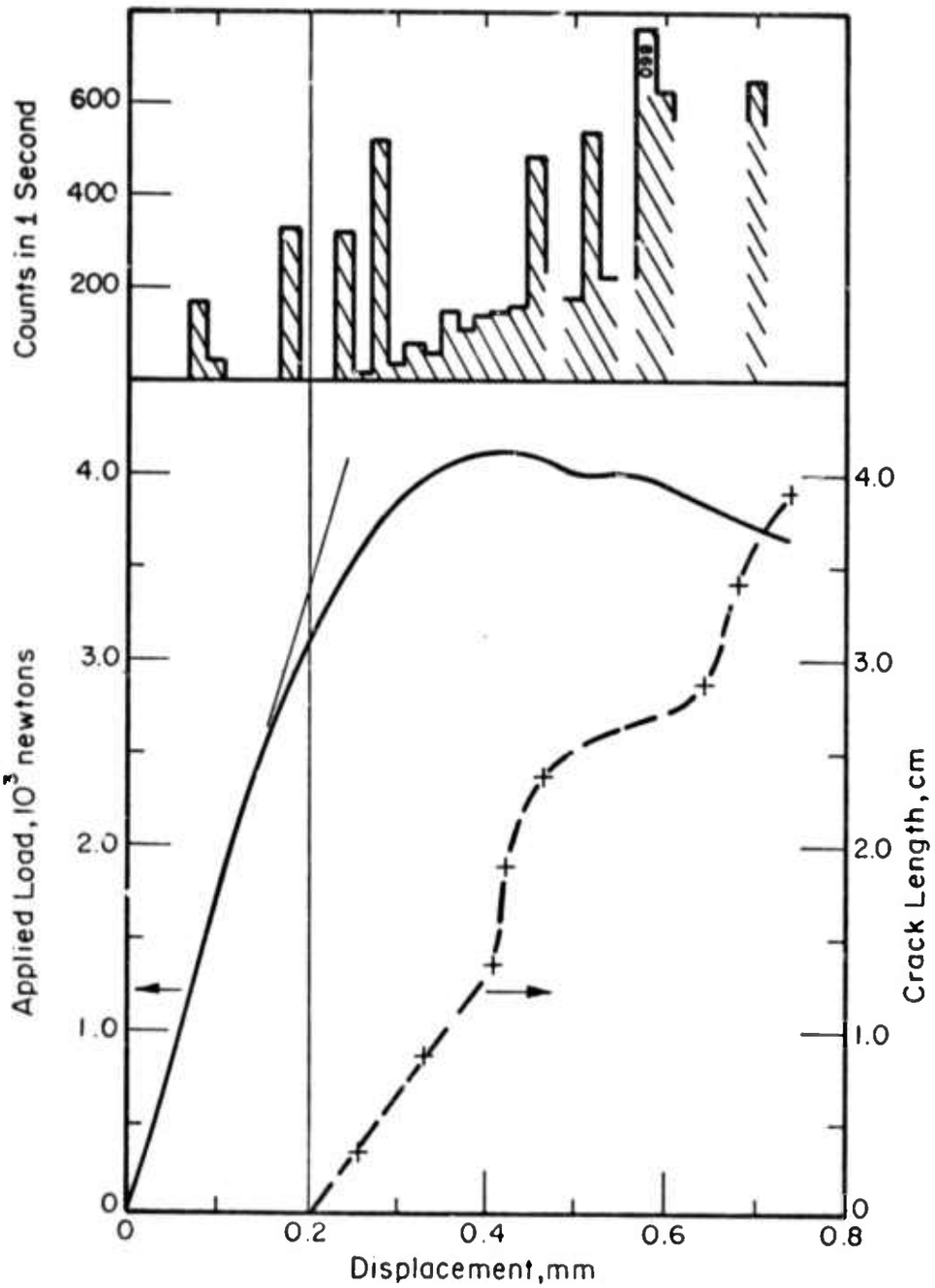

(b) Sioux Quartzite (Specimen QAX-3)

FIGURE 3. (Continued)

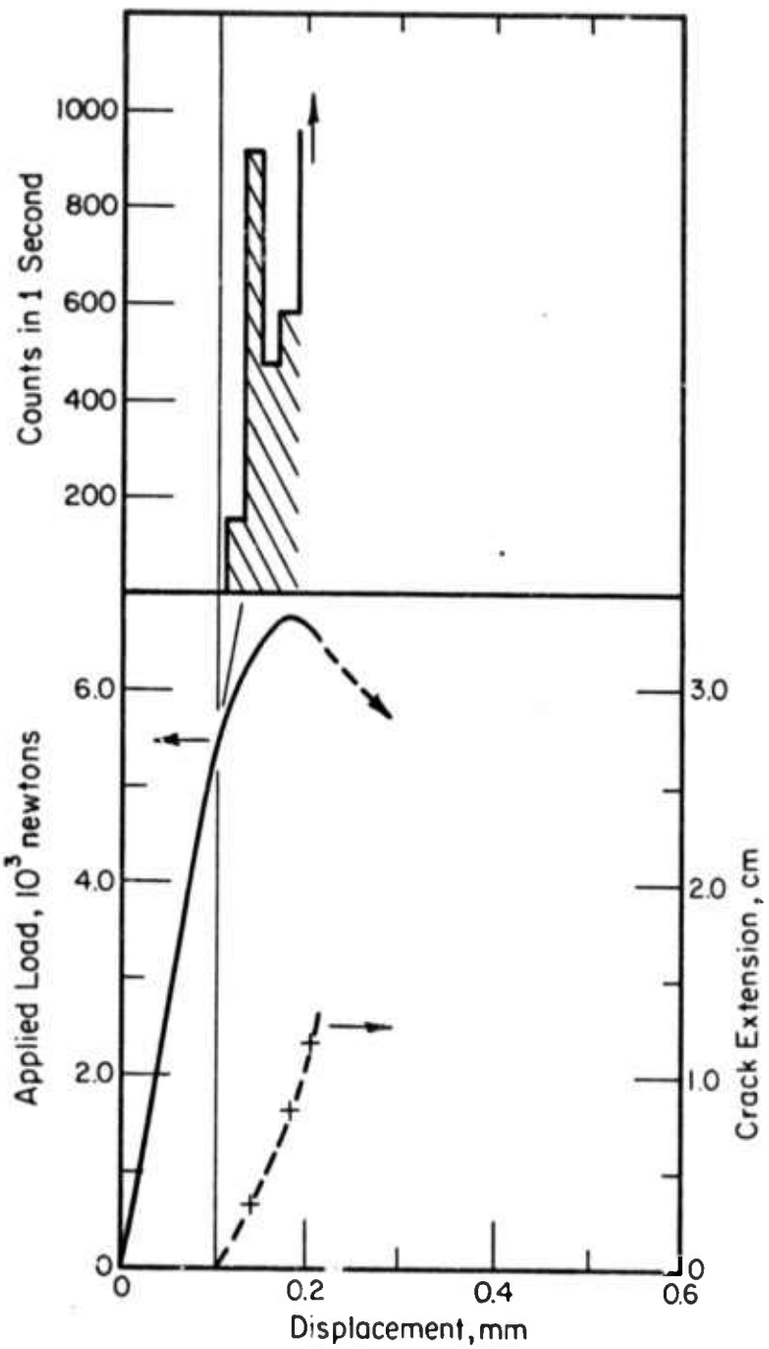

(c) Dresser Basalt (Specimen BAX-1)

FIGURE 3. (Continued)

Essentially the same behavior displayed by the granite was observed in the Sioux quartzite shown in Figure 3(b). We note some evidence here for acoustic activity prior to the point of departure of nonlinearity. During the stable crack growth stage, both the granite and and quartzite display prominent bursts of noise. These periods of relatively high acoustic activity are thought to be associated with particular regions in the rock where extensive damage by microcracking occurs suddenly and energetically. In fact, these regions may also be the source of the isolated burst of noise observed prior to extension of the main crack in these two materials. Acoustic activity prior to crack extension as shown in Figure 3(b) was observed in most but not all of the quartzite specimens.

The records obtained from the basalt specimens are very typically reproduced in Figure 3(c). No indication of microcracking activity, either from the load-displacement record or acoustic emissions, was observed prior to the onset of extension of the main crack. However, the lack of acoustic activity does not preclude microcracking since the amplitude of the pulses in this case may have been below the detection level. The point of departure from linearity in the load-displacement record and the onset of detectable acoustic activity was concurrent with the onset of crack extension in every test. Stable crack extension was typically observed for a distance of only one to two centimeters in the basalt. The crack then propagated rapidly causing one or both arms of the specimen to fracture. Failure of the specimen by fracture of the arms was prevalent in all three rocks and is likely caused by large preexisting planes of weakness or cracks. These flaws were evidently more common in the basalt, since, as indicated earlier, some specimens fell apart while they were being prepared.

For each of the three rock types, crack growth begins prior to maximum load. Therefore, at least up to the point of maximum load, the energy dissipation rate is increasing with crack length. This behavior is reflected in Figure 4 which shows examples of the variation of R with crack length for each rock tested in air at room temperature. After some crack extension the R values typically reach a relatively constant plateau, although this plateau may suddenly shift as the crack enters material with different toughness. In some cases the crack ran to the side of the specimen before the plateau level could be measured.

The R values from individual specimens are tabulated in the appendix while the results for each orientation and testing conditions are summarized in Table 2. Perhaps the most characteristic feature of the R results for all three rock types is the large degree of scatter. While the scatter makes it difficult to arrive at a definitive comparison of anisotropy or environmental effects the following inferences seem apparent:

Granite

(1) There is no evidence that the fracture energy dissipation rate depends on crack plane orientation.

(2) The R values for granite are insensitive to temperature in the range of 25°C to -196°C and show little, if any, difference between fracture in air and in the aluminum chloride solution.

Quartzite

(1) Crack propagation is most difficult in the Z (vertical) direction on the B plane.

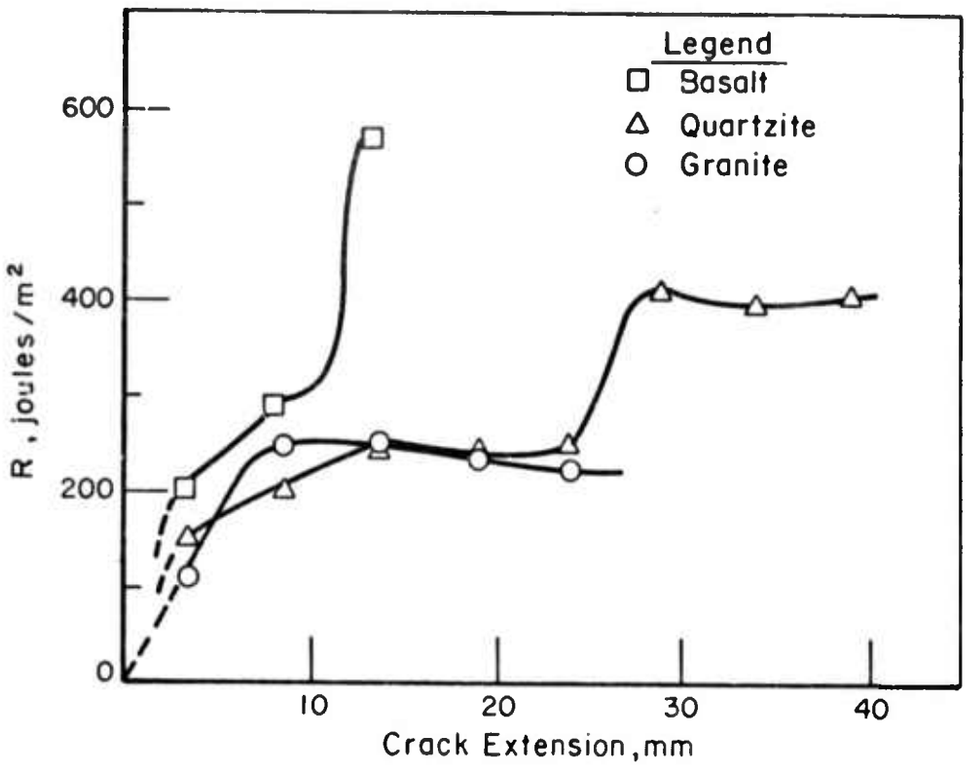

FIGURE 4. EXAMPLES OF THE VARIATIONS IN FRACTURE ENERGY DISSIPATION RATES WITH CRACK EXTENSION. These results were computed from the data in Figure 3.

TABLE 2. SUMMARY OF ENERGY DISSIPATION RATE RESULTS

Crack Plane[a]	Crack Propagation[a] Direction	Test Temperature	Environment	R[b] joules/m^2
		Barre Granite		
Rift	X	25°C	Air	183 to 338
Rift	Z	25°C	Air	(263 to 280)[d]
Grain	Y	25°C	Air	228 to 317
Hardway	Z	25°C	Air	150 to 247
Hardway	Z	25°C	$AlCl_3$[c]	278 to 294
Grain	X	-196°C	Liquid Nitrogen	217 to 247
		Sioux Quartzite		
A	X	25°C	Air	71 to 412
B	X	25°C	Air	(214)[d]
B	Z	25°C	Air	400 to 1178
C	Z	25°C	Air	264 to 441
A	X	25°C	$AlCl_3$[c]	115 to 179
B	X	25°C	Distilled Water	145 to 273
A	X	-196°C	Liquid Nitrogen	192 to 215
B	X	-196°C	Liquid Nitrogen	221 to 240
		Dresser Basalt		
A	X	25°C	Air	(571)[d]
B	X	25°C	Air	(240 to 400)
C	Z	25°C	Air	329 to 1500
A	X	25°C	$AlCl_3$[c]	(334 to 3011)[d]
B	X	25°C	Distilled Water	(368)[c]
B	X	25°C	Liquid Nitrogen	(315)[c]

(a) The range of R values obtained after the relatively constant asymptotic level was reached.

(b) 5×10^{-4} m $AlCl_3$ solution.

(c) The range of the asymptotic R level could not be defined. (See appendix)

(d) See Figure 1 for definition of plane and direction terminology.

(2) The aluminum chloride environment appears to increase R in the case of the CZ orientation but has no effect on the AX orientation. Hence, this environment effect is inconclusive.

(3) Test temperature has no discernible effect on R

Basalt

(1) The degree of variance in the R values is greatest in the basalt.

(2) Fracture along the CZ orientation is apparently most difficult.

(3) In one case, specimen BAX-3, a test in aluminum chloride solution resulted in an extremely high R value ($> 3011\ J/m^2$). However, this value could not be reproduced. This may indicate that the fracture of certain constituents in the basalt is environmentally sensitive and can be detected only if the crack tip enters these constituents, although examination of the specimens did not reveal any differences in the microstructural properties of specimen BAX-3 compared to the other specimens.

(4) No temperature effect is apparent.

Fractography

An example of the crack profile in the granite is shown in Figure 5. It is obvious that the crack seeks the most frangible constitutents, in this case, mica. At relatively low magnifications, there is no evidence that the microstructure adjacent to the crack contains more damage than in regions far from the crack. At higher magnifications, details of the various

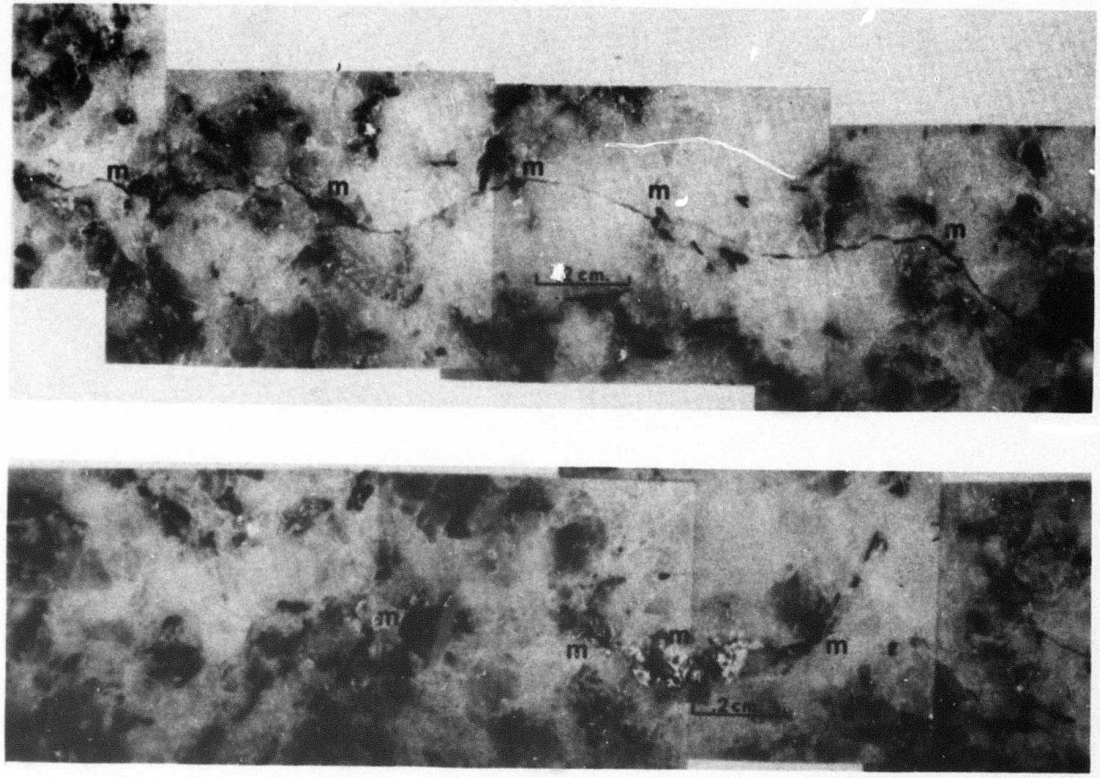

FIGURE 5. CRACK PROFILE IN GRANITE AT LOW MAGNIFICATION. The slot tip is on the right side in the upper photograph and the crack runs from right to left, ending at the extreme left side of the lower photograph. (m identifies micas intersected by the crack)

fracture modes become apparent although it was not possible to relate the local microscopic fracture appearance to the underlying constitutents. Examples taken from the fracture surface of granite specimens are shown in Figure 6 (by scanning electron microscopy) and Figure 7 (by electron microscopy of two-stage replicas obtained from the fracture surface). In Figures 6(a) and (b) there is clear evidence of secondary cracks extending to the exposed fracture surface. In Figure 6(b) these secondary cracks are nearly parallel to the plane of the exposed surface which gives rise to very thin lenticular sheets. This latter type of fracture appearance was quite common and is, therefore, likely to be a feature characteristic of one of the major constitutents rather than mica. Mica also shows delamination but of a different character as shown in Figure 6(c). Note that the mica lamellae appear relatively smooth whereas the fracture in 6(b) is distinctly conchoidal. Other representative types of fracture morphologies are found in Figure 7. The smooth surfaces evident in Figure 7(a) is also indicative of mica.

A large amount of secondary microcracking is also evident on the fracture surfaces in the Dresser basalt shown in Figure 8. This splintering fracture is typical of the major portions of the fracture morphology in this material although some conchoidal features quite similar to that found in the granite were also observed.

The SEM stereo pairs provide a very distinct impression of the highly uneven relief of the fracture surface. In the previous years work on limestone and sandstone, elevation profiles of the fracture surfaces of sandstone were measured quantitatively from stereo pairs. The results of

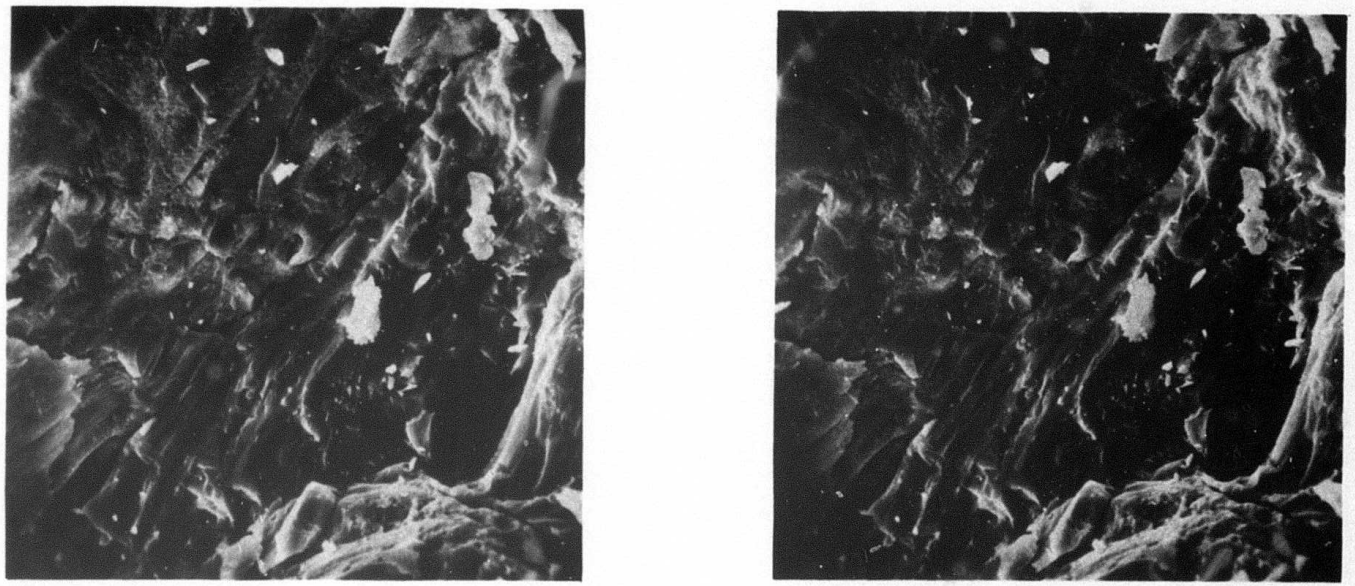

(a)

FIGURE 6. STEREO PAIRS OBTAINED BY SEM OF GRANITE FRACTURE SURFACE. (a) and (b) at 1100X, (c) at 5400X.

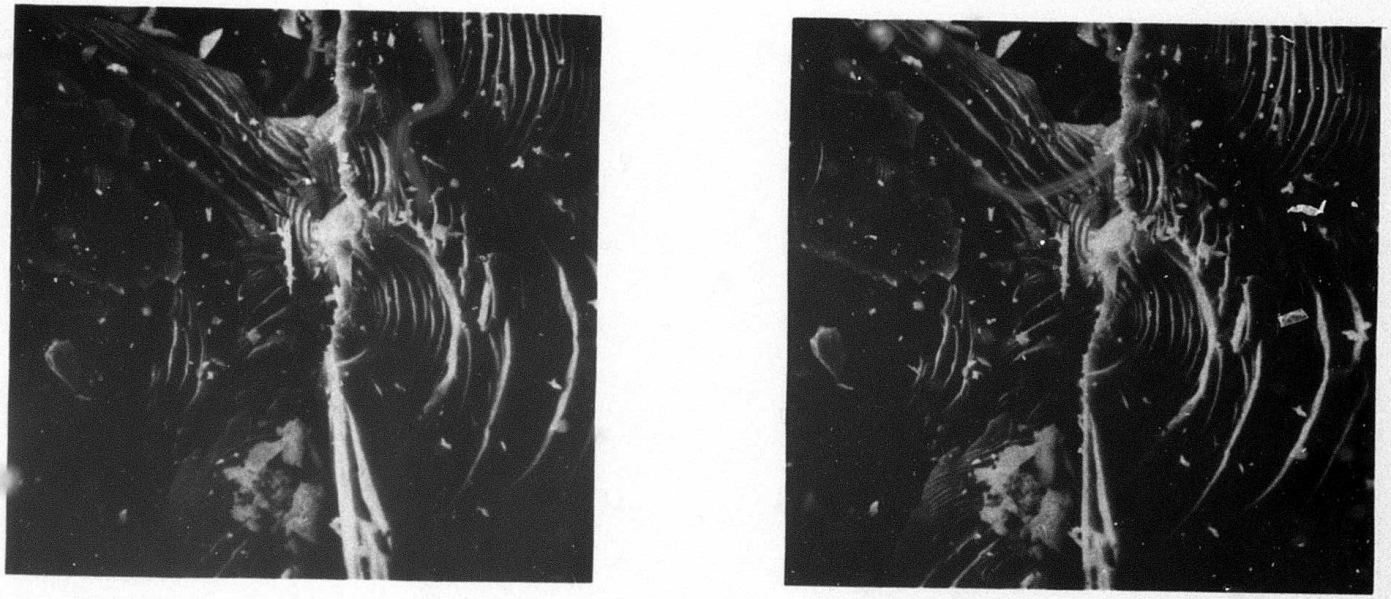

(b)

FIGURE 6. (Continued)

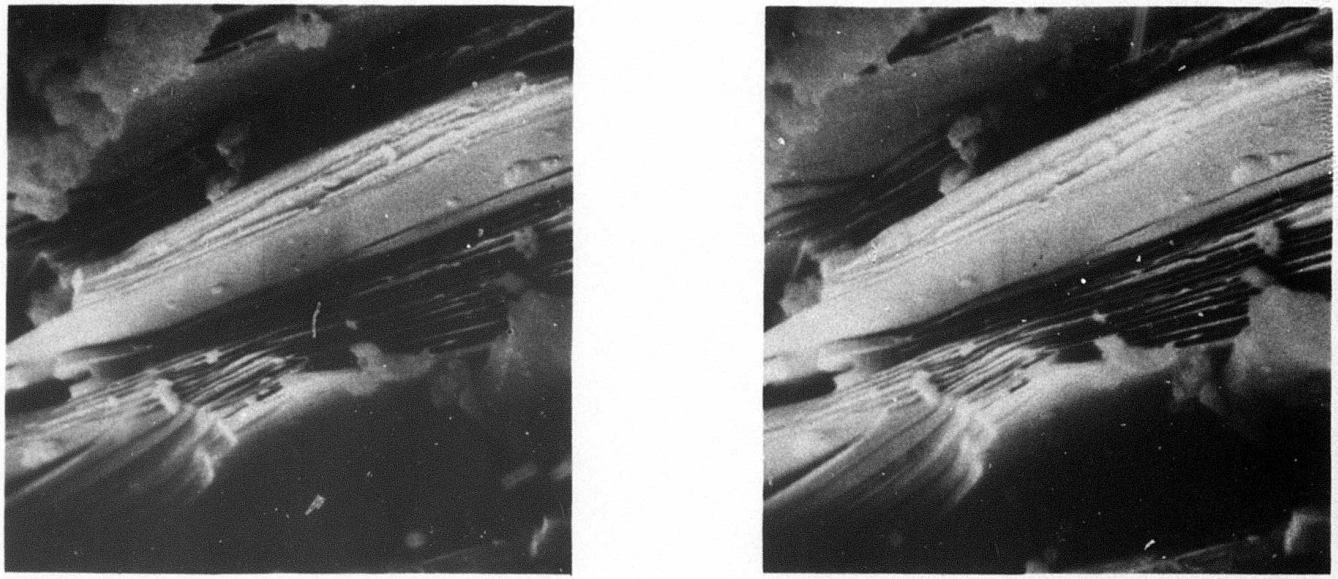

(c)

FIGURE 6. (Continued)

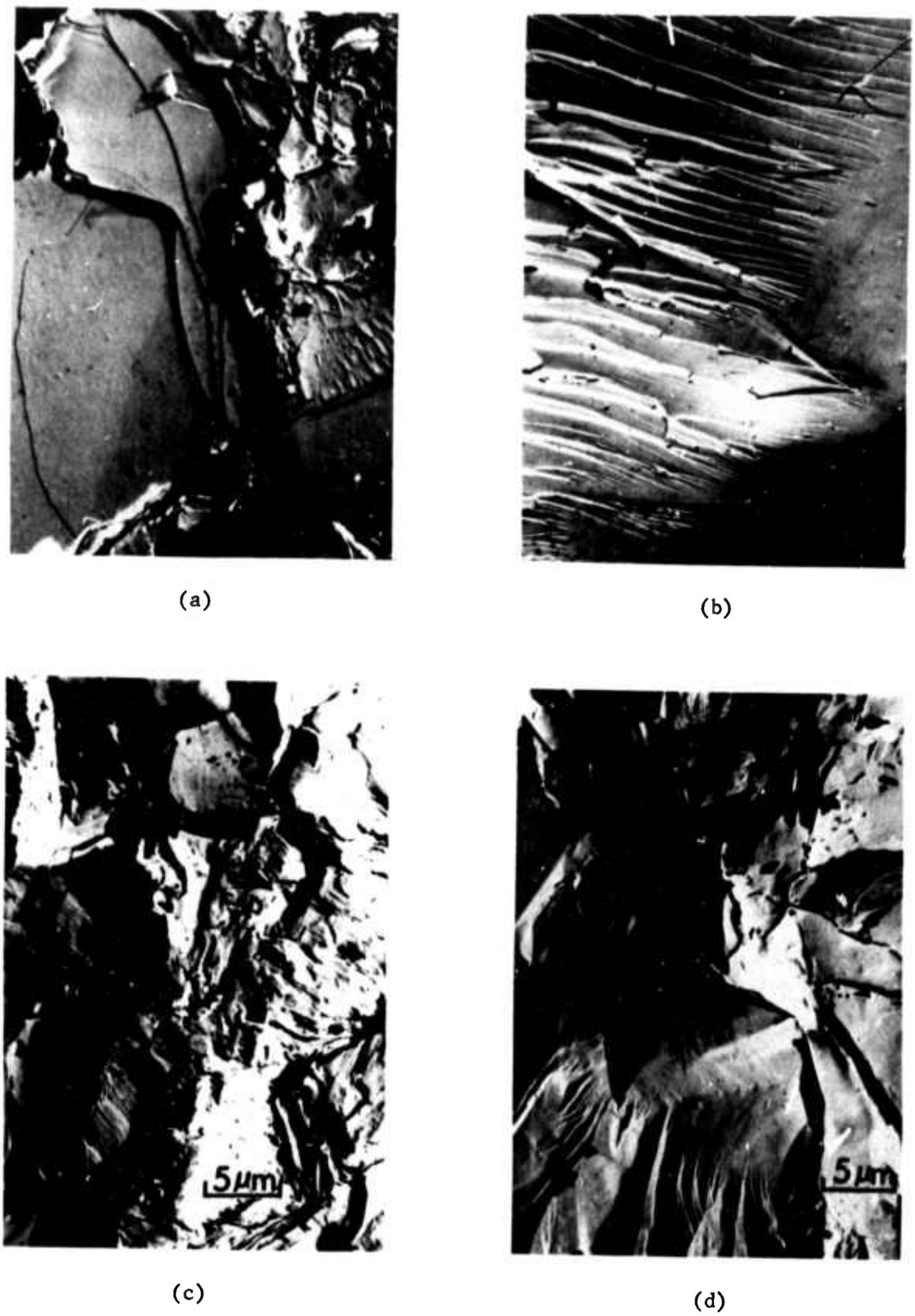

FIGURE 7. ELECTRON MICROSCOPE FRACTOGRAPHS OF Pt-C SHADOWED REPLICAS FROM THE FRACTURE SURFACE OF GRANITE.

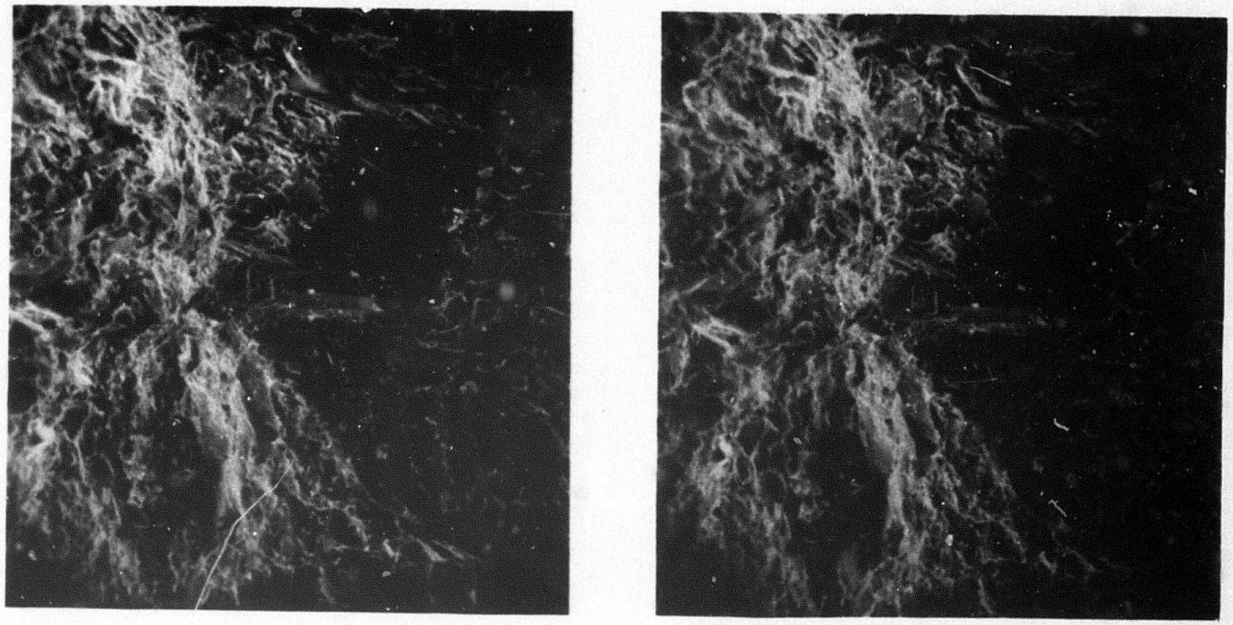

(a)

FIGURE 8. SEM STEREO PAIRS OF BASALT FRACTURE SURFACE. Magnification (a) 670X, (b) 2600X. The area in (b) corresponds to the center of the area in (a).

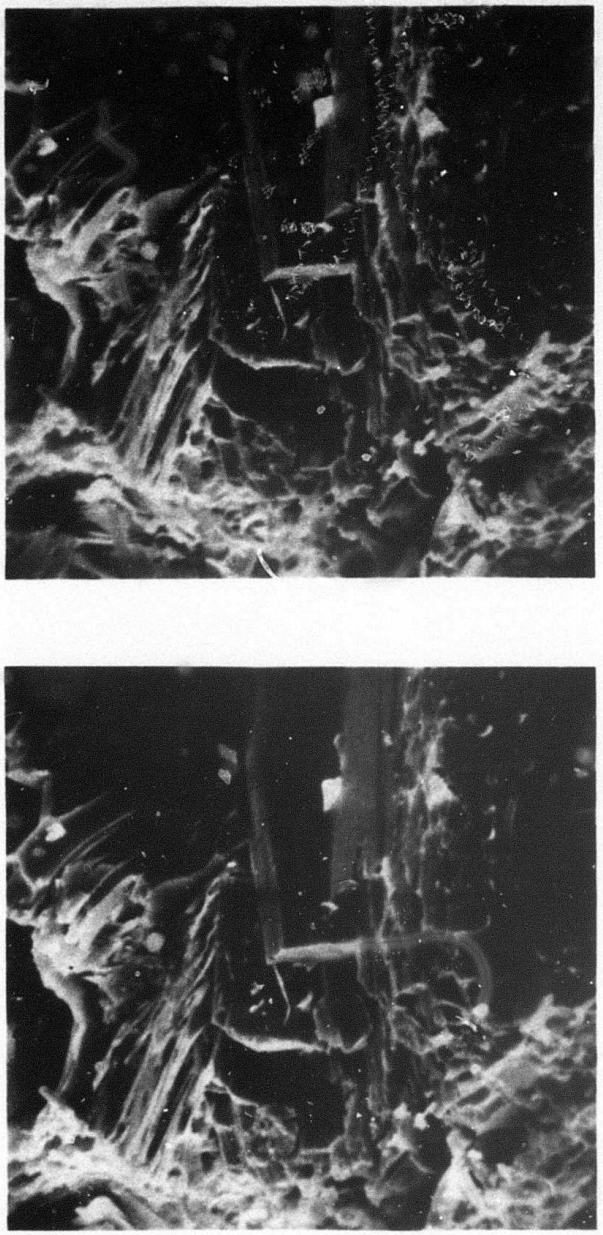

FIGURE 8. (Continued)

these measurements indicated that the area of the exposed fracture surface on this material was approximately 11 times the projected surface area. While profiles were not measured on the granite or basalt, there are at least qualitative similarities in the topological relief of the fracture surfaces of these materials and the sandstone. We would estimate that the order of magnitude difference between the exposed surface area and the projected area is applicable to the granite and basalt.

Effect of Specimen Size on R

The possibility exists that the microcrack damage zone surrounding the main crack tip is so large in the sandstone that it influences the procedure for calculating R from the crack-length displacement records. This effect was examined using specimens whose dimensions differed by a factor of two in width and length but had the same thickness (1.5 cm). The results are given in Table 3. The specimen orientations given in Figure 1 for the Sioux quartzite apply to the sandstone.

A comparison of the AY orientation for the two specimen sizes indicates that a small size dependence exists. The direction of the effect is to decrease R with increasing specimen size. This effect is analogous to results often found in fracture toughness testing of tough metals, i.e., a plastic zone which occupies a substantial part of the specimen volume leads to errors which accentuate the measured crack-opening displacement in the specimen. This leads to a calculated R which is too large, and as the specimen size is increased (relative to the plastic zone), the apparent R at fracture decreases. An alternative explanation might be derived from flaw statistics theories, e.g., Weibull theory[10]. In essence, this predicts

TABLE 3. EFFECT OF SPECIMEN SIZE ON R IN BEREA SANDSTONE

Specimen Size	Crack Plane	Crack Propagation Direction	R (joules/m^2)
25.0 x 14.7 x 1.5 cm	A	Y	175-210
	C	Z	295-480
17.8 x 7.8 x 1.5 cm	A	Y	202-259
Previous Years Results[2,3]			
17.8 x 7.8 x 1.5 cm	A	Y	465-520
	C	Z	1120-1580

simply that increasing the volume of a test specimen increases the probability for finding large flaws (or larger than some prescribed size) within the test volume. However, the volume of "test material" in these specimens may appropriately be defined by some locus around the crack tip and which depends on the applied load. Thus, at equivalent loads the test volume in both DCB specimens is identical and, therefore, flaw statistics theories would be inappropriate.

In contrast to the size effect, a very large difference is seen in comparing this year's results with the previous years which was obtained from a different block of Berea sandstone. This factor of two-to-three variation in R between these two blocks is indicative that over distances larger than a foot the toughness of the rock may vary significantly. Unfortunately, the relative location of these two blocks in the quarry is not known.

DISCUSSION

The intrinsic R values for the consituents of these rocks are likely to be of the order of 1-4 J/m^2[†]. Therefore, relative to the projected fracture area, the measured fracture energies are roughly 100 times greater than the expected intrinsic values. Since the actual exposed surface area is approximately 10 times the projected area, the irregularity of the exposed surface does not appear to be sufficiently great to offer a plausible explanation of the measured energy dissipation rates. On the other hand, several observations made during the tests support the view that

---

† Intrinsic surface energies, γ, for several oxides have been reported, e.g., for Quartz, γ = 0.4-1 J/m^2(11), for MgO, γ = 1.2 J/m^2(12); for Muscovite, γ = 0.4 J/m^2(13). Since R accounts for total energy dissipated in forming two surfaces, the intrinsic R = 2γ.

microcracking occurs prior to fracture and further that the energy dissipated in forming this additional surface area may be the dominant contribution to the fracture energy. The following evidence may be cited:

(1) Nonlinear Compliance. During loading of the granite and quartzite, the load-displacement records become nonlinear prior to both maximum load and onset of crack extension. The production of microcracks is consistent with this behavior since they must decrease the effective elastic modulus of the test specimens. In contrast, the basalt exhibited a linear load-displacement record up to the time of the onset of crack extension.

(2) Acoustic Emissions. In the cases of granite and quartzite, bursts of acoustic activity occurred prior to onset of crack extensions of the main crack and nearly coincident with the occurrence of the deviations from linearity in the specimen compliance. These emissions are a strong indication of microcracking activity, although other microscopically catastrophic events, such as twinning, cannot be entirely ruled out. We should also point out that the discontinuous behavior of the acoustic activity prior to crack extension in these two rocks is not entirely consistent with a very gradual departure from linearity in the load-displacement record. As noted earlier these bursts of noise are likely produced by the particularly energetic formation of microcracks in certain regions of the rock and that significant amounts of additional microcracking may be producing noise which is below our detection level. In view of this, the lack of acoustic activity in the early stage of the tests in the basalt does not rule out the possibility that microcracking is occurring in this material.

(3) Environment Independence. The Rehbinder effect has been used to advantage to increase drilling rates by the addition of certain agents to the flushing liquid[14]. Also significant decreases in the tensile strength of quartzite have been observed in aqueous solution containing more than 400 ppmw $AlCl_3$[15]. Other examples of environmentally induced decreases in fracture energy of ceramics can be found[16]. All of these effects have been interpreted in terms of a surface reaction at the tips of critical flaws causing either a reduction in the surface free energy or increased resistance to crack-tip plastic deformation. In view of this we should reasonably expect similar decreases in the fracture energy of the granite, quartzite, and basalt if, indeed, the fracture energy of these materials is dissipated principally at the main crack tip which is exposed to the environment. The fact that little or no effect of environment (between air, $AlCl_3$ solutions, and liquid nitrogen) was detected suggests instead that the fracture energy is dissipated in regions inaccessible to the environment. The creation of nonconnecting microcracks in a volume in the vicinity of the main crack tip is a mechanism consistent with this observation.

(4) Fractography. Fracture surfaces in Figures 6 and 7 indicate secondary microcracking emerging at the exposed fracture surface. However, the possibility remains that these cracks were present in the material prior to testing.

(5) Observations in Similar Materials. Extensive microcracking prior to tensile failure has been observed directly in quartzite by Friedman, et al[17], and in concrete my Moavenzadeh and Kugel[18]. Microcracking provided the explanation for the large R values measured by the authors[2,3] during fracture of limestone and sandstone. More recently,

microcrack generation has been advanced as the principal mechanism producing high R values in very hard polycrystalline ceramics such as zirconia[19] and hafnium titanate[20].

In the previous work, analysis of the limestone and sandstone results suggested a model which allowed an estimation of the total area created by microcracking at the onset of fracture. In this model the DCB specimen was treated simply as two cantilever beams anchored to a rigid foundation and a further simplifying assumption was made that the formation of a microcrack of length 2c decreases the effective elastic modulus of the material (increases the specimen compliance) by the same amount as in a center cracked sheet. Using these assumptions the following expression for total microcrack area results:

$$A = \frac{b^2 ha}{4\pi\alpha}\left[1 - \frac{5}{4} + \frac{S}{3}\ln\frac{3(S-2)}{2S} + \frac{S^2}{18(S-2)}\right], \qquad (3)$$

where b = specimen thickness

a = main crack length

h = specimen beam height

α = average area per microcrack (C^2).

The parameter S depends on the ratio of tensile strength of the rock to the nominal applied stress at the notch tip,† and may be derived in two ways. In the first case, we assume that the tensile strength of the rock is exceeded at the notch tip at the load, P_c, corresponding to the onset of deviation from linearity. Then from simple beam theory we derive that at loads greater than P_c,

$$S_1 = \frac{6P_c}{P} \qquad (4)$$

---

† In the previous report S was defined as $S = \frac{6\sigma_c a}{\sigma}$, where σ_c is the tensile strength of the rock, a is the crack length, and σ is the nominal bending stress at the crack tip which is obtained by idealizing the DCB specimen as a pair of cantilever beams anchored to a rigid foundation. Here we redefine S to be $S = 6\sigma_c / a\sigma$.

Alternatively, we may use the measured tensile strength of the rock, σ_c, and express the nominal stress at the crack tip in terms of the measured R value. In this case we obtain

$$S_2 = 2\sigma_c \sqrt{\frac{3h}{ER}} \tag{5}$$

Denoting the bracketed terms on the right in Equation (3), by the symbol, F, the rates of formation of microcrack area per unit area of main crack becomes simply:

$$\frac{dA}{bda} = \frac{bh}{4\pi\alpha} F \quad . \tag{6}$$

We have calculated typical values for F from Equation (4) at maximum load using the records in Figure 3 and also from Equation (5) using the data from the corresponding specimens given in the appendix. These results are contained in Table 4. The agreement between the two methods for determining F and also between the values of F for the granite and quartzite is very good. While the assumptions made in computing F provide little confidence in its magnitude, this agreement supports the concept on which the calculation is based, i.e., a sizable region surrounds the crack tip in which the tensile strength of the rock would be exceeded if microcracks could not form. The magnitude of the average microcrack area in the granite and quartzite is not known but may be estimated from Equation (6) if it is assumed that the areal rate of microcrack formation is about 100 times greater than the projected fracture surface area. Thus, taking b = 16 mm, h = 38 mm, and F = 0.05, we obtain $\alpha \sim 0.024 \times 10^{-6}\ m^2$ giving an average microcrack dimension of about 0.16 mm. This figure must be regarded as a

TABLE 4. EVALUATION OF THE MICROCRACK FORMATION RATE PARAMETER, F

(Specimen)	P_c, 10^3 Newtons	$P^{(a)}_{(max)}$ 10^3 Newtons	F (by Equation (4))	σ_c (b) Mn/m^2	R J/m^2	F (by Equation (5))
Granite (GHZ-2)	2.1	2.8	0.052	7.67	220	0.055
Quartzite (QAX-3)	3.1	4.1	0.050	10.8	250	0.053
Basalt (BAX-1)	5.5(c)	6.6	0.037	22.1	550	(d)
Limestone(e)	-	-	0.079	3.58	50-230	(d)
Sandstone(e)	-	-	0.142	-	-	-

(a) Maximum load.

(b) Tensile strength data provided by Krech, Reference 7.

(c) Deviation from linear load-displacement behavior occurred at the onset of crack extension. This behavior suggests that the nominal stress at the notch did not exceed the tensile strength.

(d) The model breaks down because $S < 2$. This suggests that the nominal stress at the notch tip is more than three times the measured tensile stress.

(e) Data for limestone and sandstone taken from Reference (2). The value of F calculated by Equation (4) for these two materials was obtained from Table 3 in Reference 2.

rough order of magnitude estimate of the microcrack size, although it compares reasonably well with the average grain size in the granite and quartzite.

The Dresser basalt does not display the strong evidence for microcracking as the granite or quartzite. Yet the fracture energy value for this material tends to be significantly greater. The linearity up to crack extension indicates that the crack tip damage zone, if it exists, is much smaller in the basalt than the granite or quartzite. In addition as can be seen in Table 4, the two methods used to calculate F for basalt are in strong disagreement. Equation (4) predicts very little nonlinearity, while Equation (5) suggests that the tensile strength of this material is greatly exceeded by the nominal crack tip stress during crack propagation. In the latter case this result is similar to that found for the limestone. We see no reason at this time to conclude that the constituents of the basalt should have a greater tendency to undergo plastic deformation than the granite or quartzite. Thus, while the basalt results are inconclusive we favor the interpretation that microcracking is the dominant energy dissipation mechanism in this material and that it occurs by the creation of an extremely dense population of microcracks in a relatively small region surrounding the main crack tip. The alternative conclusion is that the flow stress of the constituents of the basalt is sufficiently low that large amounts of energy is dissipated by dislocation generation and glide or possibly by twinning.

The lack of anisotropy in R also indicates that the ease of forming microcracks under load bears little relation to the preferred orientation of preexisting flaws. This appears to be particularly evident

in Barre granite. In this material Douglas and Voight[6] report that the largest proportion of identifiable interfaces and cracks are oriented with their poles normal to the rift plane, followed closely by the fraction of poles normal to the grain, and the smallest fraction with poles normal to the hardway plane. This preferred orientation of preexisting flaws correlates well with the anisotropy in Young's modulus for this material; i.e., smallest modulus perpendicular to the rift and largest perpendicular to hardway. In contrast, R for Barre granite shows no distinct anisotropy. Thus, it seems likely that while preexisting flaws may act as nuclei for the formation of microcracks in the vicinity of the main crack tip they are not sufficiently dense to aid the propagation of a crack parallel to the rift relative to the hardway.

The small, but detectable, effect of specimen size on fracture energies in sandstone underscores the importance of designing an experiment which yields material properties results not influenced by the experiment itself. In this case, by increasing the specimen size the relative fraction of the specimen occupied by the nonlinear damage zone is decreased. One consequence is that the size of the damage zone becomes less influenced by the nearby free edges of the test specimen, and also the calculation of R, which assumes the specimen material to behave linearly elastic throughout, becomes more accurate. Because the size of the damage zone decreases with either increasing strength or decreasing toughness, this effect should be less important in the tests of granite, quartzite, and basalt and should not be a factor in the R values for these materials. However, we expect that the relevance of these fracture energies to rock breakage operations is also dependent on the general state

of stress involved. Specifically, the measured fracture energies for Barre granite, Sioux quartzite, and Dresser basalt are material properties appropriate to tensile fracture. Thus, operations, such as blasting, which involve the propagation of cracks over considerable distances under the action of tensile stresses will involve energy consumptions defined by the product of R and the surface area created. On the other hand, fracture by shear, or where large components of hydrostatic compression are present, may involve significantly different fracture energy dissipation rates. Thus we would not expect a direct relation between R and the energy consumption in drilling.

CONCLUSIONS

The wedge-loaded, double-cantilever-beam technique was successfully applied to the measurement of fracture energy, R, in Barre granite, Sioux quartzite, and Dresser basalt, although some problems occurred due to the tendency for asymmetric fracture of the specimens. The results indicate that for the granite and quartzite, microcracking is the dominant energy dissipating mechanism and leads to values of R which are roughly 100 times greater than intrinsic surface-free energies of the constitutents.

The values of fracture energy obtained from basalt are very strongly scattered but, in some cases, exceed those R values obtained from the granite and quartzite. The results do not provide a clear indication of the mechanism for dissipating energy during fracture but the microcracking model is favored.

The R for the granite shows no anisotropy with orientation of the crack plane although predominant fractions of preexisting flaws are oriented parallel to the rift and, to a lesser extent, the grain planes. It, therefore, appears that while preexisting flaws may act as microcrack nucleation sites they are not sufficiently dense to aid crack propagation.

Finally, the fracture energy dissipation rates were measured in this study under tensile opening stresses (Mode I) and are applicable directly only to those rock breakage operations where the predominant crack driving force is also supplied by tensile stresses.

ACKNOWLEDGMENT

This research was supported by the Advanced Research Projects Agency of the Department of Defense and was monitored by Bureau of Mines under Contract No. H0220066.

REFERENCES

(1) C. Fairhurst, Estimation of Mechanical Properties of Rock Masses, Final Report on ARPA-USBM Contract H0220011, Univ. of Minnesota (1973).

(2) R. G. Hoagland, G. T. Hahn, and A. R. Rosenfield, Rock Mech., 5, 77 (1973).

(3) R. G. Hoagland, G. T. Hahn, A. R. Rosenfield, R. Simon, and G. D. Nicholson, Influence of Microstructure on Fracture Propagation in Rock, Final Report, on ARPA-USBM Contract H0210006, Battelle, Columbus Laboratories (1972).

(4) F. Moavenzadeh and R. Kuguel: J. of Materials, 4, 497 (1969).

(5) M. Friedman, J. Handin, and G. Alanis: Technical Report No. 4 to Dept. of the Army, Texas A & M Univ., College Station, Texas (1971).

(6) P. M. Douglass and B. Voight, Geotechnique, 19, 376 (1969).

(7) W. W. Krech, Personal Communication. Information taken from "A Standard Rock Suite for Rapid Excavation Research", by W. W. Krech, F. A. Henderson, and K. E. Hjelmstad, Proposed BuMines IC.

(8) M. F. Kanninen, Int. J. Fract., 9, 83 (1973).

(9) R. G. Hoagland, Trans ASME, Series D, 89, 525 (1967).

(10) W. Weibull, Proceedings, Royal Swedish Instr. Engr. Res. No. 151 (1939).

(11) W. F. Brace and J. B. Walsh, Am. Mineralogist, 47, 1111 (1962).

(12) J. J. Gilman, J. Appl. Phys., 31, 2208 (1960).

(13) J. W. Obreimoff, Proc. Roy. Soc. London, A, 127, 290 (1930).

(14) P. A. Rehbinder, L. A. Schreiner, and K. F. Zhigach, Hardness Reducers in Drilling, Acad. of Sciences, Moscow, USSR, trans by CSIR, Melbourne (1948).

(15) V. S. Vitukuri, Trans AIME, 252, 407 (1972).

(16) S. M. Weiderhorn, Int. J. Frac. Mech., 4, 171 (1968).

(17) M. Friedman, J. Handin, and G. Alani, Technical Report No. 4 to Dept. of Army, Texas A & M Univ., College Station, Texas, September 15, 1971.

(18) F. Moavenzadeh and R. Kuguel, J. of Materials, 4, 497 (1969).

(19) D. J. Green, P. S. Nicholson, and J. D. Embury, Microstructural Development and Fracture Toughness of a Calcia Stabilized Zirconia, J. Am. Ceramic Soc., in press.

(20) R. G. Hoagland, C. W. Marschall, and A. R. Rosenfield, The Strength and Fracture Energy of Hafnium Titanate, presented at 1973 ASM Materials Engineering Congress, Chicago, 1-4 October.

TABLE A-1. COMPILATION OF ENERGY DISSIPATION RATE RESULTS

Specimen Identification	Crack Plane[a]	Crack Propagation Direction[a]	Test Temperature	Environment	Asymptotic R_2 ($joules/m^2$) Variation[b]	Mean
			Barre Granite			
GRX-1	Rift	X	25°C	Air	216-255	233
GRX-2	Rift	X	25°C	Air	183-338	254
GRZ-1	Rift	Z	25°C	Air	> 280	
GRZ-2	Rift	Z	25°C	Air	263-276	270
GGY-1	Grain	Y	25°C	Air	268-317	300
GGY-2	Grain	Y	25°C	Air	> 228	
GGX-1	Grain	X	-196°C	Liq. Nitrogen	217-247	230
GHZ-1	Hardway	Z	25°C	Air	150-223	190
GHZ-2	Hardway	Z	25°C	Air	222-247	237
GHZ-4	Hardway	Z	25°C	$AlCl_3$[c]	278-294	284
			Sioux Quartzite			
QBZ-1	B	Z	25°C	Air	700-1178	940
QBZ-2	B	Z	25°C	Air	> 404	
QBZ-3	B	Z	25°C	Air	> 484	
QAX-2	A	X	25°C	Air	71-74	73
QAX-3	A	X	25°C	Air	240-412	327
QAX-4	A	X	25°C	$AlCl_3$	115-179	140
QAX-1	A	X	-196°C	Liq. Nitrogen	192-215	203
QBX-4	B	X	25°C	Air	> 257	
QBX-5	B	X	25°C	Air	> 214	
QBX-3	B	X	25°C	Distilled Water	145-273	188
QBX-2	B	X	-196°C	Liq. Nitrogen	221-240	230
QCZ-2	C	Z	25°C	Air	> 312	
QCZ-3	C	Z	25°C	Air	264-441	377
QCZ-1	C	Z	25°C	$AlCl_3$	495-554	526

(Continued)

TABLE A-1. (Continued)

Identification	Crack[a] Plane	Crack Propagation[a] Direction	Test Temperature	Environment	Asymptotic R (joules/m^2) Variation[b]	Mean
			Dresser Basalt			
BCZ-1	C	Z	25°C	Air	329-381	349
BCZ-2	C	Z	25°C	Air	1406-1506	1456
BBX-1	B	X	25°C	Air	> 240	
BBX-2	B	X	-196°C	Liq. Nitrogen	> 315	
BBX-3	B	X	25°C	Dist. H_2O	> 368	
BBX-4	B	X	25°C	Air	> 400	
BBX-5	B	X	25°C	Air	363-398	380
BAX-1	A	X	25°C	Air	> 571	
BAX-2	A	X	25°C	$AlCl_3$	334-375	360
BAX-3	A	X	25°C	$AlCl_3$	> 3011	

(a) See Figure 1.

(b) The range of R values obtained after the relatively constant asymptotic level was reached. Cases where the crack propagated out of the midplane of the specimen before the asymptotic level was reached are denoted by " > " symbol.

(c) 5×10^{-4} m $AlCl_4$ solution.